



LAWRENCE  
LIVERMORE  
NATIONAL  
LABORATORY

# ALE3D Simulation of Incompressible Flow, Heat Transfer, and Chemical Decomposition of Comp B in Slow Cookoff Experiments

M. A. McClelland, E. A. Glascoe, A. L. Nichols, S. P. Schofield, H. K. Springer

June 23, 2014

International Detonation Symposium  
San Francisco, CA, United States  
July 13, 2014 through July 18, 2014

## **Disclaimer**

---

This document was prepared as an account of work sponsored by an agency of the United States government. Neither the United States government nor Lawrence Livermore National Security, LLC, nor any of their employees makes any warranty, expressed or implied, or assumes any legal liability or responsibility for the accuracy, completeness, or usefulness of any information, apparatus, product, or process disclosed, or represents that its use would not infringe privately owned rights. Reference herein to any specific commercial product, process, or service by trade name, trademark, manufacturer, or otherwise does not necessarily constitute or imply its endorsement, recommendation, or favoring by the United States government or Lawrence Livermore National Security, LLC. The views and opinions of authors expressed herein do not necessarily state or reflect those of the United States government or Lawrence Livermore National Security, LLC, and shall not be used for advertising or product endorsement purposes.

## ALE3D Simulation of Incompressible Flow, Heat Transfer, and Chemical Decomposition of Comp B in Slow Cookoff Experiments

Matthew A. McClelland, Elizabeth A. Glascoe, Albert L. Nichols III,  
Samuel P. Schofield, and Harry K. Springer

Energetic Materials Center, Lawrence Livermore National Laboratory  
Livermore, CA 94551

**Abstract.** An ALE3D thermal-fluids model was developed for Comp B (63% RDX, 36% TNT, 1% wax) and applied to a Scaled-Thermal-Explosion-eXperiment (STEX) with slow heating. Solubility and viscosity models were developed for a well-mixed RDX-TNT slurry. Chemical kinetics parameters for a one-step Prout-Tompkins model were obtained using One-Dimensional-Time-to-Explosion (ODTX) measurements and a non-linear regression routine. In the application of the thermal-fluids model, the strong convection of mass, momentum, and energy was reduced at high temperatures and associated low slurry viscosities to make the simulations numerically tractable. The ODTX thermal-fluids simulations show that in the fast experiments, flow reduces explosion times and self-heated liquid rises to the top of the cavity and ignites. The STEX model shows that flow leads to a small delay in the explosion time and ignition near the top of the vessel. Model comparison with STEX thermocouple measurements, suggests RDX settles in the slurry to form a solid-like material in the lower portion of the vessel and a more fluid material above.

### Introduction

Slow cookoff is of interest in the areas of fire hazard reduction, and key questions concern explosion time and violence. Low melting point explosives such as Comp B, TNT, and PETN can exhibit behavior significantly different than solid explosives due to the formation and flow of liquid-solid and all liquid phases. This flow can increase the thermal transport by orders of magnitude, changing the ignition time and location along with the violence.

In the early cookoff models for Comp B, solid RDX and TNT decompose to gaseous products. Tarver and McGuire<sup>1</sup> developed a 1D model with

thermal transport and multi-step kinetics to represent Comp B ODTX measurements (see Fig. 1). This model was refined by Zerkle<sup>2</sup> to give better agreement with experiment.

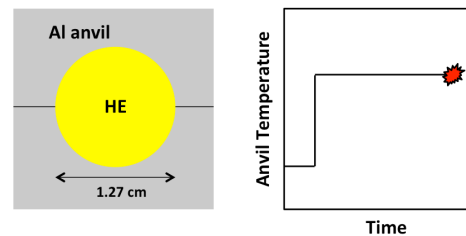


Fig. 1. ODTX layout and boundary conditions.

An ALE3D cookoff model was used to simulate the thermal, chemical, and mechanical behavior during the heating and explosive phases of a Comp B STEX experiment (TE-012)<sup>3,4</sup> (see Fig. 2). Although the model provided a satisfactory prediction for the explosion temperature, it did not capture some of the fluid-like behavior seen in an internal thermocouple trace.

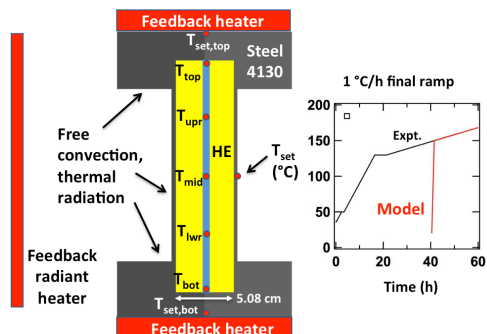


Fig. 2. STEX layout and boundary conditions.

Here we model the buoyancy-driven flow, thermal convection, and species transport along with chemical decomposition in this same Comp B STEX test using capabilities recently added to the ALE3D modeling framework<sup>5</sup>. The effects of flow are explored and results for explosion time and temperature fields are compared with ODTX and STEX measurements.

### ALE3D Thermal-Fluids Model

An ALE3D thermal-fluids is being developed to model the flow, thermal, and species transport, along with chemical decomposition in cookoff. The model composition is taken to be 64% RDX, 36% TNT, with the wax neglected. In this incompressible flow model, a single reactant decomposes into a product species with the same material properties. Gases generated by decomposition and evaporation are assumed to move rapidly to the top of the HE vessels and not influence the flow and decomposition. This relatively simple model allows the effects of flow mechanics to be more readily investigated.

### RDX Solubility in TNT

The solid-liquid phase behavior has a strong influence on the viscosity of the mixture. TNT melts at 81°C and forms a slurry with RDX particles (see Fig. 3). RDX dissolves in the liquid as the temperature increases towards the RDX melting point of 205°C.

For model development, solubility measurements<sup>6</sup> are extrapolated from near the eutectic point to the RDX melting point using the following expression for the liquidus weight fraction (see Fig. 3 and Table 1):

$$\omega = a_0 + a_1T^* + a_2T^{*2} + a_3T^{*3} \quad (1)$$

$$T^* = (T - T_{mp,TNT}) / (T_{mp,RDX} - T_{mp,TNT}) \quad (2)$$

Here it is assumed that no intermediate compounds are formed and that the mixture is at equilibrium. These assumptions are less valid as the temperature and decomposition rate increase. One important consequence of Eq. (1) is that the 64 wt% RDX in the Comp B is completely dissolved in the liquid at a temperature of 185°C.

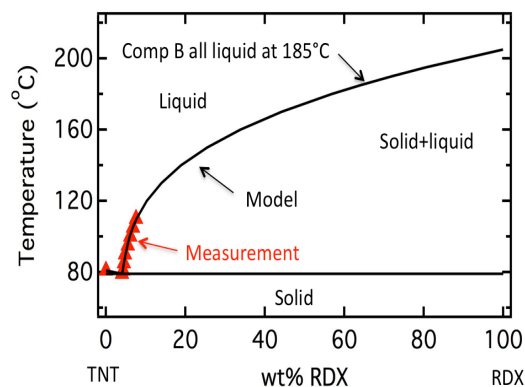


Fig. 3. Model RDX-TNT phase diagram.

### Heat of Dissolution and Thermal Properties

Differential Scanning Calorimetry (DSC) curves for Comp B, RDX, and TNT are used to help assess the solubility curve (Eq. (1)) and estimate the heat of dissolution (see Fig. 4). The DSC curves give the heat flow resulting from phase change and decomposition as the samples

are heated at 10°C/min. The Comp B and TNT peaks at 81°C show the endothermic heat flows associated with the melting of TNT in the Comp B and TNT samples. The RDX curve shows two peaks at 190 and 200°C, which are likely related to the  $\beta \rightarrow \delta$  phase transition of contaminant HMX and the RDX melting.

Table 1 Comp B material parameters

Par.	Value	Par.	Value
a0	0.0426	$T_{mp,RDX}$	81°C
a1	0.0753	$T_{mp,TNT}$	205°C
a2	0.1340	$\Delta H_{sol}$	$1.05 \times 10^5$ J/kg RDX
a3	0.7474	$C_{p,tot}$	1780 J/kg-°C
$\varphi_0$	0.827	k	0.246 W/m-°C
$T_\mu$	3388 K	$\ln(\mu_{s0})$	-13.74 Pa-s
m	1	$\rho_0$	1690 kg/m <sup>3</sup>
n	1	d $\rho$ /dT	-0.675 kg/m <sup>3</sup> -°C
$T_0$	478 K	E/R	27,000 1/K
p	6	$\ln(A_0)$	-2.80 1/s
		$\Delta H_{rxn}$	$5.02 \times 10^6$ J/g

The Comp B shows a heat of dissolution as the temperature increases from 90 to 185°C. An estimate for the heat of RDX dissolution was calculated as 67 J/g of Comp B (105 J/g of RDX dissolved) based on the area under the curve. For this estimate, the baseline was aligned with low temperature measurements between 45 and 60°C and included a heat flow area between 90 and 110°C consistent with the above solubility data (see Fig. 3). The baseline was adjusted so that the integral of this heat flow relative to the total heat of dissolution matched the fraction of RDX dissolved.

Although replicate runs yielded heats within 1 J/g, the results are quite sensitive to the placement of the baseline and have uncertainties greater than 10%. One contribution to this uncertainty is the overlap between the dissolution region and the exothermic decomposition region at temperatures above 185°C. Finally, it is noted that this value of 105 J/g of RDX dissolved is less than 161 J/g for the RDX heat of fusion<sup>1</sup>.

A model heat flow curve for dissolution of RDX in the Comp B sample was calculated based on Eq. (1), a constant value of 105 J/g of RDX dissolved, and the assumption of instantaneous

equilibrium (see Fig. 4). The model and measured Comp B heat flow are similar at lower temperatures, but diverge near the temperature of 185°C for complete dissolution.

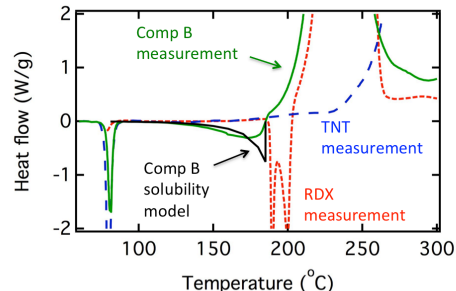


Fig. 4. DSC heat flows for Comp B, RDX, and TNT at a ramp rate of 10 °C/min.

Finally, it is observed that the DSC curves for RDX and TNT cannot be combined simply to give the Comp B curve. The RDX in Comp B dissolves at temperatures below 185°C rather than melts all at once 205°C (see Fig. 4). Also, the Comp B decomposes in a single peak rather than in two separate peaks as would result from the simple combination of the RDX and TNT curves. Thus, separate RDX and TNT decomposition reaction sequences cannot be simply combined to give the Comp B behavior.

For this initial thermal-fluids model, the heat of solution 67 J/g, a TNT heat of fusion of 94 J/g, and the average sensible heat of 1.24 J/g-°C were combined into single average heat capacity (see Table 1). The temperature range for averaging was 20-205°C. A single average thermal conductivity was also assigned for this temperature range.

Model density curves are shown in Fig. 5 for Comp B, RDX, and TNT. Comp B is treated as an ideal material in which the densities are simply combined with no density change of mixing. However, it is likely that the TNT liquid with dissolved RDX would have a higher density than the simple combination of the solid RDX and liquid TNT densities used in this study.

In this thermal-fluids model, we use a model with linear temperature dependence, which is fit to the densities in the solid-liquid region between 81 and 205°C (see Table 1). We employ the

Boussinesq approximation in which the temperature-dependent density  $\rho$  is used in the buoyancy driving force term, but is constant at the 20°C value of  $\rho_0=1.69 \text{ g/cm}^3$  in all other terms.

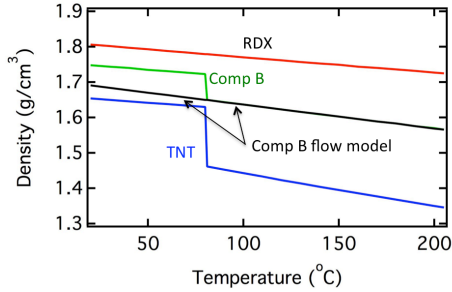


Fig. 5. Model density for Comp B, RDX, and TNT

### Viscosity

A viscosity curve for the slurry and all-liquid phase was developed for a well-mixed Comp B slurry sample at the bulk composition (see Fig. 6). Measurements at three temperatures were made by Nunez et al.<sup>7</sup> between 85 and 135°C. The one-parameter Mooney equation<sup>8</sup>, developed for a suspension of spheres, was used to represent the viscosity of the slurry:

$$\mu_{\text{eff}}/\mu_s = \exp[2.5\phi/(1 - \phi/\phi_0)] \quad (3)$$

in which  $\phi$  is the solid volume fraction,  $\phi_0$  is the value at maximum packing, and the  $\mu_s$  is the temperature-dependent RDX-TNT solvent viscosity.  $\phi$  is calculated as a function of temperature using the solubility curve (Eq. (1)) and the density curves of Fig. 5 at the bulk composition. The solvent viscosity is estimated from viscosity measurements of TNT<sup>9</sup> and the following expression

$$\mu_s = \mu_{s0} \exp(T_\mu/T) \quad (4)$$

The parameter  $\phi_0$  was adjusted to give the best representation of the measurements<sup>9</sup>. The resulting slurry viscosity decreases by a factor of 1000 from 81 to 185°C. Note that the viscosity curve (Eq. (3)) can be applied at other compositions, or with sedimentation models, since

it is only a function of  $\phi$ , and has no explicit dependence on temperature.

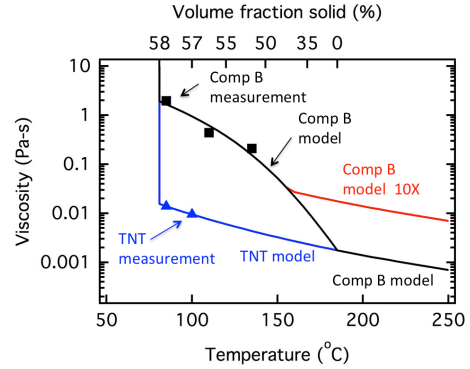


Fig. 6. Measured<sup>7,9</sup> and model Comp B and TNT viscosity curves.

### Chemical Decomposition

The decomposition of the Comp B is represented by a single-step Prout-Tompkins (PT) Arrhenius expression<sup>10</sup>

$$\frac{d\omega}{dt} = -A_0 \exp\left[-\frac{E}{R}\left(\frac{1}{T} - \frac{1}{T_0}\right)\right] \omega^n (1 - q\omega)^m \quad (5)$$

in which

- $\omega$  = mass fraction of reactant
- $A_0$  = frequency factor
- $E$  = the activation energy
- $R$  = universal gas constant
- $T$  = temperature
- $T_0$  = reference temperature
- $n, m, q$  = kinetics parameters

It is also convenient to define

$$p = -\log_{10}(1-q) \quad (6)$$

The parameters  $E/R$ ,  $A$ , and  $p$  were adjusted with  $m=n=1$  to fit ODTX measurements as described below. The parameter  $p$  generates a characteristic time delay for the reaction of the scale  $p/A_0$  for  $m=n=1$ . The parameter  $m$  has a strong effect on reaction progress in the early stages of the reaction when  $\omega \sim 1$ , while  $n$  is

important for progress during the later stages of the reaction when  $\omega \sim 0$ .

The measured ODTX explosion times in this study provide data for the end time of thermal decomposition, but no information related to the earlier progress of the reaction. Consequently, we set  $m=n=1$ . Finally it is noted that most ODTX reactions do not progress very far with  $\omega < 10\%$  before thermal runaway, ignition, and explosion.

### Species Diffusivity

Although the reactant and product species are taken to have identical properties, the mass diffusivity  $D_{AB}$  is important for two reasons. First, the inter-diffusion of the reactant and product slows the reaction rate Eq. (5), which can be seen when it is written in an autocatalytic form. Second, liquid diffusivities are of the scale  $1 \times 10^{-5} \text{ cm}^2/\text{s}$ <sup>8</sup> and sufficiently small to generate numerical instabilities for the flows of this study. Here the mass diffusivity is set at constant values large enough to avoid these instabilities as is described in the next section (see Table 2).

Table 2 Characteristic quantities and dimensionless groups for ODTX and STEX simulations

	ODTX	STEX
T (°C)	220	155
D (cm)	1.27	5.08
$\rho$ (g/cm <sup>3</sup> )	1.69	1.69
$\mu$ (Pa-s)	$1.04 \times 10^{-2}$	$3.42 \times 10^{-2}$
$\gamma_\alpha$ (s/cm)	4.07	4.07
$k_{sw} = k(1 + \gamma_\alpha v)$ (W/m-°C)	0.376	0.446
$C_p$ (J/g-°C)	1.78	1.78
$D_{AB}$ (cm <sup>2</sup> /s)	$1 \times 10^{-3}$	$5 \times 10^{-3}$
v (cm/s)	0.13	0.20
Re = $\rho v D / \mu$	2.68	2.51
$Pe_\alpha = \rho C_p v D / k_{sw}$	132	343
$Pe_D = v D / D_{AB}$	165	102

### Numerical Strategies

#### Thermal-Fluids

ALE3D<sup>5,11</sup> was used to solve the 2D axisymmetric time-dependent (1) mass and momentum equations for incompressible flow, (2) thermal and species transport equations, and (3)

the decomposition reaction Eq. (5). The velocity, temperature, and species profiles were represented by linear finite elements and the time integration method employed implicit and explicit terms. A fast iterative solver, GMRES, was generally used to solve the matrix, but a full-matrix decomposition was performed for some of the most challenging high-temperature ODTX simulations.

Since the time integration strategy included an explicit component, a Courant condition was used to limit the time-step size in order to maintain stability and accuracy:

$$\Delta t = Co \Delta x / v_{max} \quad (7)$$

Here  $\Delta t$  is the time-step size,  $\Delta x$  is a characteristic element dimension, and  $v_{max}$  is the maximum flow speed. The Courant number,  $Co$ , was set at a value of 0.1.

Several strategies were employed to handle the strong flows, thermal, and species convection, combined with the multi-hour cookoff times in the STEX and longer ODTX experiments. In order to keep computational times manageable in terms of the number of time steps, viscosities at the higher temperatures were increased by 10X (see Fig. 6) to reduce the flow velocity and increase the time-step size following Eq. (7).

In order to maintain numerical stability for the thermal convection of this low diffusivity explosive of this study, a term with coefficient  $\gamma_\alpha$  was added to the standard conduction term to provide additional thermal diffusion in the flow direction where it is needed<sup>12</sup>:

$$\mathbf{q} = -k(\boldsymbol{\delta} + \gamma_\alpha \mathbf{v}\mathbf{v} / |\mathbf{v}|) \cdot \nabla T \quad (8)$$

Here  $\mathbf{q}$  is the heat flow vector,  $\mathbf{v}$  is the velocity vector,  $|\mathbf{v}|$  the magnitude, and  $\boldsymbol{\delta}$  is the unit tensor. The added thermal diffusion in the flow direction is zero for a liquid at rest, and increases linearly with the flow velocity. There is no added diffusion in the direction normal to flow. It can be shown the Peclet number, a dimensionless measure of convection, approaches a maximum of

$$Pe = \rho C_p D / (k \gamma_\alpha) \quad (9)$$

In order to avoid spurious oscillations in a 1D steady-state convective-diffusion problem with linear finite elements

$$Pe < 2n_x \quad (10)$$

Here  $n_x$  is the number of zones in the flow direction<sup>13</sup>. Although this same algorithm will soon be implemented for species transport, the mass diffusivity  $D_{AB}$  was increased by trial and error to a level where numerical stability could be achieved (see Table 2).

Since the number of time steps ranged from  $10^5$  and  $10^6$  for the multi-hour ODTX and STEX simulations, respectively, meshes were kept relatively coarse. For the 2D ODTX, meshes had between 864 and 7776 elements, while the STEX meshes had between 2640 and 5997 elements.

#### Chemical Kinetics Parameters by Regression

The kinetics model parameters were determined by applying non-linear regression with the reaction (Eq. (5)) and the 1D heat conduction model for the ODTX. For ODTX modeling, the parameters  $A_0$ ,  $E/R$ , and  $p$  are adjusted with  $m=n=1$ . The value for the reference temperature  $T_0=205^\circ\text{C}$  was selected to be in the middle of the temperature range to make the changes in the parameters  $A_0$  and  $E/R$  as orthogonal as possible.

The nonlinear regression is performed using the Frontline Solver routine with a VBA function incorporating an efficient solution algorithm for the 1D thermo-chemical model. A second-order finite difference method was employed in space, and a Trapezoid Rule with automatic step-size control was used for the time integration. Coarse uniform meshes with as few as 20 zones were sufficient to obtain accurate explosion times in the simulation of multi-hour experiments, whereas meshes with as many as 400 zones were needed to resolve the behavior in thin boundary layers for short experiments of the scale 10 seconds.

#### ODTX Measurements and Model

The influence of flow on Comp B ODTX results is explored using the above thermal-fluids model and numerical strategy (see Fig. 1). In Fig.

7, the measured explosion times are plotted versus temperature for the Comp B sample of interest.

#### Chemical Kinetics Parameters from ODTX

First the chemical kinetics parameters in Eqs. (5) and (6) were determined using the 1D thermo-chemical model with no species diffusion and the above non-linear regression procedure. The parameters  $A_0$ ,  $E/R$ , with  $m=n=1$  and  $p=6$  were adjusted to give the parameters in Table 1 and the explosion times in Fig. 7. The value for  $p$  was not allowed to go higher than 6 in an attempt to avoid possible difficulties with numerical noise in the second bracketed “delay” term of Eq. (5). This delay term is very small at the beginning of decomposition.

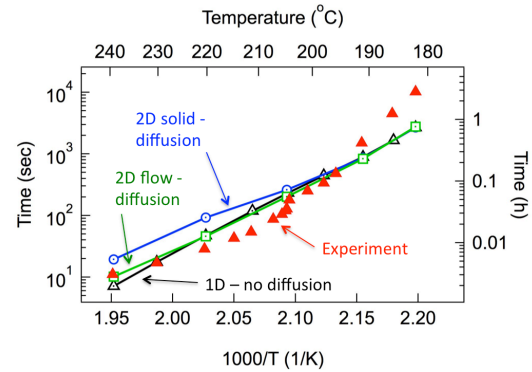


Fig. 7. Model and measured ODTX explosion temperatures for Comp B.

The resulting 1D thermo-chemical model with PT kinetics provides a fair representation, but does not capture the curvature of the explosion time measurements (see Fig 7).

The effect of convective flow and species diffusion in the ODTX system is evaluated with the 2D axi-symmetric thermal-fluids model. As mentioned above, the high temperature liquid viscosities were increased by as much as 10X (see Fig. 6) to make the simulations computationally tractable by reducing the flow velocities and number of time steps, following the Co condition (Eq. (7)). Thermal diffusion was applied in the flow direction using Eq. (8) to maintain numerical stability in the presence of strong thermal convection. The value of  $\gamma_\alpha$  in Table 2 was used to keep the maximum Pe no. below the value of 400

based on Eq. (9). For the species diffusivity, a value of  $1 \times 10^{-3} \text{ cm}^2/\text{s}$  was selected to maintain numerical stability, which is approximately the same as the thermal diffusivity of  $8.2 \times 10^{-4} \text{ cm}^2/\text{s}$  calculated from properties given in Table 1.

The 2D thermal-fluids explosion times are compared at five temperatures in Fig. 7 with the measurements, 1D results with no diffusion, and 2D results with diffusion and no flow.

At the lower temperatures between 182 and 205°C, all of the models give nearly the same explosion times. There is good agreement with measurement at 205°C, but large differences at the lowest temperatures. The similarity of the model results indicates that flow and species diffusion have little influence on the explosion time at the lower temperatures. For all of the models, the Comp B reaches the boundary temperature after approximately 300 s, which is of the same scale as the thermal diffusion time

$$t_\alpha = R^2/\alpha = (0.635 \text{ cm})^2/(8.2 \times 10^{-4} \text{ cm}^2/\text{s}) = 492 \text{ s}$$

After this initial heating phase, the Comp B stays at a uniform temperature for hundreds of seconds until self-heating occurs. These cases with long explosion times are particularly useful for understanding chemical kinetics, since the effect of transport processes is relatively small. It is also noted that coarse meshes with 25 elements in a coordinate direction can be used since gradients in flow, temperature, and concentration fields are small for much of the simulation.

At the highest temperatures of 220 and 239°C and the shortest explosion times, the influence of flow and transport is strong. Comparing the model explosion times for the no-flow cases with (2D) and without diffusion (1D), shows that inter-diffusion of the reactant and product increases the explosion times by more than 2X. The addition of diffusion gives no-flow explosion times higher than the experimental values.

Comparing the 2D flow and no-flow cases with diffusion shows that the effect of flow is to reduce the explosion times by  $\sim 2\text{X}$  at 220 and 239°C. Thermal convection of the Comp B near the anvils increases the rate at which the Comp B is heated, leading to the smaller explosion times. These results are in approximate agreement with the measurements.

Buoyancy effects also cause the self-heated liquid to rise and ignition to occur near the top of the cavity (see Fig. 8) in contrast to the no-flow case, which ignites in a ring near the boundary.

It is noted that in order to resolve the strong gradients in thin boundary layers, we used the finest meshes with grading and as many as 80 elements in a coordinate direction. A 50% increase to this number of element changed the explosion time by less than 5% at the highest temperature of 239°C.

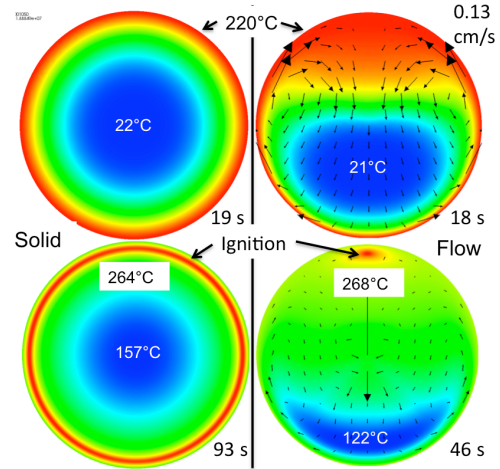


Fig. 8. ODTX temperature and velocity fields for flow and solid models with diffusion at 220°C.

For the wall temperature of 220°C, the flow intensity and strength of thermal and species convection is indicated with the calculation of the Reynolds and Peclet numbers shown in Table 2. Here the 10X viscosity at 220°C was employed (see Fig. 6) along with the streamwise diffusivity at the characteristic velocity of 0.13 cm/s. It is seen that the simulated flow is laminar with  $Re=2.68$ , which is less than a characteristic laminar-turbulent transition value of 1000. The thermal and species convection is strong with Pe values 132 and 165, respectively. The meshes are of the size needed to handle the flows since the Pe nos are of the same scale as the number of elements in a coordinate direction (see Eq. (10)).

## STEX Measurements and Model

The above thermal-fluids model for Comp B was applied to a STEX test TE-012<sup>3</sup> (see Fig. 2). A 646 g charge of Comp B was poured into a 4130 steel vessel with a diameter of 5.08 cm, length of 20.32 cm, and wall thickness 0.406 cm. Approximately 10% ullage at room temperature was included to allow thermal expansion without pressure burst prior to ignition. The 2 kbar confinement was maintained using metal O-rings bolted between flanges. Three radiant heaters spaced at 120° provided the energy to heat the sides of the while two independent resistance heaters were used to heat the top and bottom flanges of the assembly. The temperature fields were measured and controlled as described below, and the violence was characterized with strain gauge and radar measurements.

The temperature was measured at five internal locations using a probe and many external locations using RTDs (see Fig. 2). Three Proportional-Integral-Derivative (PID) controllers were used to keep thermocouples at top ( $T_{set,top}$ ), bottom ( $T_{set,bot}$ ), and side ( $T_{set}$ ) locations near their set-point values. In this test, the final ramp rate was 1°C/h, in which  $T_{set,bot}$  and  $T_{set,top}$  were kept 4 and 9°C lower than  $T_{set}$  in an attempt keep the ignition point near the center of the vessel. The top temperature was kept the coldest to counter the higher outside air temperatures near the top of the vessel, resulting from free convection.

The 2D thermal-fluids model is applied with the boundary conditions of Fig. 2. No ullage is included in this incompressible flow model since Comp B likely expanded to fill the initial gap at the measured ignition temperature  $T_{set}=160^\circ\text{C}$  based on the density changes shown in Fig. 5. The thermal boundary model included the above three PID temperature controllers along with air heat transfer coefficients<sup>14</sup>. The heat transfer coefficient along the side of the vessel decreases with elevation to account for heating of the air as it rises. In order to save computation time, the model set-point point  $T_{set}$  was increased from 20 to 150°C in one hour in contrast to the 1°C/h ramp from 130°C used in the experiment (see Fig. 2).

Model flow and temperature fields for the STEX experiment show the effects of strong thermal convection and buoyancy during the ramp ( $T_{set}=155^\circ\text{C}$ ) and just before ignition ( $T_{set}=168^\circ\text{C}$ ) (see Fig. 9). At  $T_{set}=155^\circ\text{C}$ , the large temperature

gradients and flow velocities of the scale 0.2 cm/s indicated strong thermal convection as the warm liquid near  $T_{set}$  rises towards the top flange at the cooler temperature of 146°C. The cooled liquid sinks along the axis of symmetry. Although all of the Comp B is molten, the flow is considerably weaker in the lower half of the vessel since cool liquid near the lower flange ( $T_{set,bot}=151^\circ\text{C}$ ) does not tend to rise.

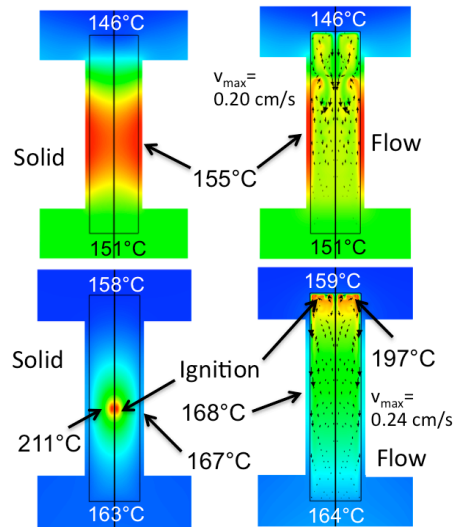


Fig. 9. STEX temperature and velocity fields for flow and solid models.

The calculation of the dimensionless groups in Table 2 shows the flow intensity and strength of thermal and species convection. Here the 10X viscosity at 155°C was employed (see Fig. 6) along with the streamwise diffusivity at 0.2 cm/s. It is seen that the simulated flow is laminar with  $Re=2.51$ , and the thermal and species convection is strong. The meshes are marginal since  $Pe_a$  is larger than 20, the number of elements in a coordinate direction (see Table 2 and Eq. (10)).

Near ignition, liquid is heated rapidly by decomposition and rises to the top of the vessel where it ignites (see Fig. 9). In contrast results for a 2D solid model show self-heating and ignition near the center of the vessel. In the solid model buoyancy forces cannot drive hot material upwards.

Temperatures at three internal TC locations are compared in Figs. 10, 11, and 12 for the experiment, the solid model, and flow model,

respectively. The internal TC measurements at  $T_{\text{upr}}$ ,  $T_{\text{mid}}$ , and  $T_{\text{lwr}}$  show self-heating as the temperatures rise above the side set-point temperature  $T_{\text{set}}$  until ignition at  $T_{\text{set}}=160^{\circ}\text{C}$ . Measured temperature rises at the center location  $T_{\text{mid}}$  are the largest and show a very smooth increase relative to  $T_{\text{set}}$  over the last 10 h. Measurements at the lower location  $T_{\text{lwr}}$  also show a smooth rise, but lag due to initially cooler temperatures. Measurements at the upper location  $T_{\text{upr}}$  are similar to  $T_{\text{lwr}}$  until  $T_{\text{set}}=152.5^{\circ}\text{C}$ . Then  $T_{\text{upr}}$  measurements approach and follow the  $T_{\text{set}}$  ramp with fluctuations, until a large increase about 5 minutes before ignition. Although both  $T_{\text{upr}}$  and  $T_{\text{mid}}$  are at similar temperatures of  $208^{\circ}\text{C}$  just prior to ignition, the rapid rise of  $T_{\text{upr}}$  suggests ignition near the top of the vessel.

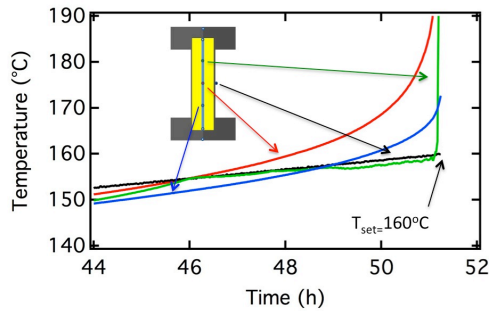


Fig. 10. STEX thermocouple measurements for Comp B.

It is seen that 2D solid model temperatures at the  $T_{\text{mid}}$  and  $T_{\text{lwr}}$  locations exhibit somewhat similar behavior to the measurements (see Fig. 11). Although the solid-model self-heating and ignition occur later when the set-point  $T_{\text{set}}$  is  $7^{\circ}\text{C}$  warmer at  $167^{\circ}\text{C}$ , the smooth temperature rises are observed with the largest increases at the center. However, near ignition, the solid model upper  $T_{\text{upr}}$  also shows a smooth temperature increase relative to  $T_{\text{set}}$ . This behavior is very different from the  $T_{\text{upr}}$  measurement, which fluctuates and follows  $T_{\text{set}}$  until the sharp rise in the last 5 min before ignition. These results suggest solid-like behavior in the middle to lower regions of the vessel, but flow and mixing in the upper portion for the vessel.

A 1D solid model without diffusion gives ignition at a lower temperature of  $166^{\circ}\text{C}$ ,

indicating that diffusion and axial heat flow in the 2D solid model slow the rate of self-heating.

For the 2D flow model, the internal temperatures  $T_{\text{upr}}$ ,  $T_{\text{mid}}$ , and  $T_{\text{lwr}}$  are all  $3^{\circ}\text{C}$  below  $T_{\text{set}}$  until one hour before ignition (see Fig. 12). During this final time period,  $T_{\text{upr}}$  rises rapidly due to self-heating and ignition occurs near the top of the vessel (see Fig. 9). Although this flow model does not capture the solid-like thermal self-heating behavior for  $T_{\text{mid}}$  and  $T_{\text{lwr}}$ , the flow model curve for  $T_{\text{upr}}$  shows the movement of the hottest liquid towards the top of the vessel similar to the experiment.

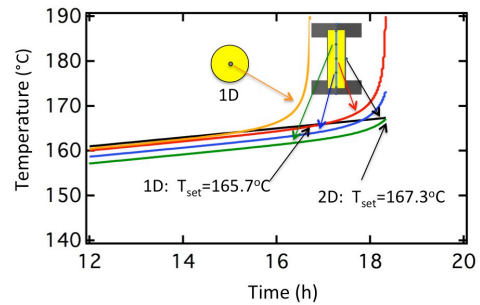


Fig. 11. Temperature predictions for STEX 2D solid model with diffusion, and 1D model without diffusion.

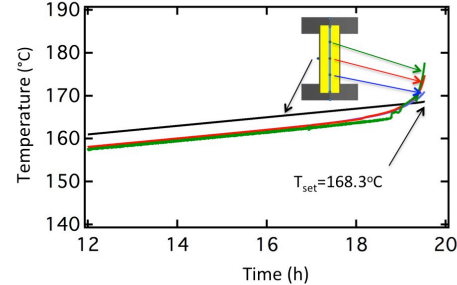


Fig. 12. STEX 2D flow model temperature predictions.

One possible explanation for the solid behavior in the middle ( $T_{\text{mid}}$ ) to lower portions ( $T_{\text{lwr}}$ ) for the vessel and more fluid-like behavior in the upper portion ( $T_{\text{upr}}$ ) of the vessel is RDX particle settling during casting and the thermal ramp. The settling of higher density RDX particles in the liquid would increase the volume fraction of solid and slurry viscosity (see Fig. 6) in

the lower portion of the vessel and leave a more fluid mixture in the upper portion of the vessel.

Finally, all of the model explosion temperatures occur at values of  $T_{set}$  which are between 6 and 8°C larger than the measured time of 160°C. The lowest model explosion temperature is 166°C for the 1D solid model, which has no species diffusion and only conduction in the radial direction at the axial mid-plane. The explosion temperature for the 2D solid model with diffusion is slightly higher at 167°C, which is followed by 168°C for the 2D flow model. Mesh refinement results for the 2D flow model give explosion temperatures within 0.2°C of the above results.

1. Despite the dramatic differences in the temperature fields (see Fig. 9), flow and diffusion do not seem to have a strong effect on explosion temperature in this slow cookoff experiment. This suggests that one important contribution to the differences between measured and model explosion times is the chemical kinetics model. Another possibility is that settling of the more thermally sensitive RDX particles to the warm center of the vessel might lead to faster decomposition and lower explosion times in the experiment than the models with uniform RDX distribution.

## Conclusions

An ALE3D thermal-fluids model including decomposition and species transport was applied to the cookoff of Comp B in ODTX and STEX experiments. Models for solubility and viscosity were developed for a well-mixed slurry of RDX particles and saturated liquid. The parameters for a one-step Prout-Tompkins kinetics model were determined from ODTX measurements using a regression procedure. For faster ODTX experiments, the thermal-fluids model shows that flow transports energy rapidly into the HE and decreases the explosion time. In contrast STEX simulations show a small increase in explosion temperature with flow. For both STEX and ODTX simulations, buoyant self-heated liquid moves the ignition location toward the upper areas of the HE. Finally, comparison with STEX 6. internal thermocouple measurements suggests RDX settling forms a highly viscous region in the

lower portion of the vessel and a more fluid material above.

## Acknowledgments

This research was partially supported by the Joint DoD-DOE Munitions Technology Development Program. This work performed under the auspices of the U. S. Department of Energy by Lawrence Livermore National Laboratory under Contract DE-AC52-07NA27344.

## References

1. McGuire, R. R. and Tarver, C. M., "Chemical Decomposition Models for the Thermal Explosion of Confined HMX, TATB, RDX, and TNT Explosives" Proceedings of the 7<sup>th</sup> Symposium on Detonation, Annapolis, MD (1980).
2. Zerkle D. K., "Composition B Decomposition and Ignition Model" Proceedings of the 13<sup>th</sup> International Detonation Symposium, pp. 771-777, Norfolk, VA (2006).
3. McClelland, M. A., Maienschein, J. L. and Nichols, A. L., "Joint DoD/DOE Munitions Technology Development Program FY-01 Progress Report, Ignition and Initiation Phenomena: Cookoff Violence Prediction" Lawrence Livermore National Laboratory Report, 2002.
4. McClelland, M. A., Maienschein, J. L., Reaugh, J. E., Tran, T. D., Nichols, A. L. and Wardell, J. F., "ALE3D Model Predictions and Experimental Analysis of the Cookoff Response of Comp B" Proceedings of JANNAF 39th Combustion and 21st Propulsion Systems Hazards Subcommittee Meetings, Colorado Springs, CO (2003).
5. Nichols A. L. and Schofield S. P., "Modeling the Response of Fluid/Melt Explosives to Slow Cookoff" Proceedings of the 15<sup>th</sup> International Detonation Symposium, submitted, San Francisco, CA (2014).

6. Federoff, B. T. and Sheffield, O. E., *Encyclopedia of Explosives and Related Items*, Picatinny Arsenal, Dover, NJ, Rept. No. Patr-2700, Vol. III, pp. c611-c621 (1966).
7. Nunez, M. P., Zerkle, D. K. and Zucker J. M. "The rheology of molten Composition B" Los Alamos National Lab Report LA-UR-12-24029 (2012).
8. Bird, R. B, Stewart, W. E., and Lightfoot, E.N., *Transport Phenomena*, Wiley (2002).
9. Drimmer, B. E., *Navy Bank of Explosives Data*, Naval Surface Weapons Center, Dalgren, VA Rept. No. NSWC MP 83-230 Vol. III, p. 4 (1983).
10. Wemhoff, A. P., Howard, W. M., Burnham, A. K. and Nichols A. L. III, "An LX-10 Kinetic Model Calibrated Using Simulations of Multiple Small-Scale Thermal Safety Tests", *J. Phys. Chem. A*, Vol 112, pp. 9005-9011 (2008).
11. Nichols, A. L., "Users Manual for ALE3D An Arbitrary Lagrange/Eulerian 3D Code System," Lawrence Livermore National Laboratory, Rpt. No. LLNL-SM-650174 (2014).
12. McClelland, M. A., "Application of Streamwise Diffusion to Time-Dependent Free Convection of Liquid Metals" *Int. J. Numer. Methods Fluids*, pp. 1061-1071, McGraw-Hill (1994).
13. Finlayson, B. A., *Nonlinear Analysis in Chemical Engineering*, pp. 240-241, McGraw-Hill (1980).
14. Holman, J. P., *Heat Transfer*, pp. 253-54, McGraw-Hill (1976).